

Observations of counter-propagating Alfvénic and compressive fluctuations in the chromosphere *

Zi-Xu Liu, Jian-Sen He and Li-Mei Yan

School of Earth and Space Sciences, Peking University, Beijing 100871, China; jshept@gmail.com

Received 2013 March 3; accepted 2013 August 15

Abstract Recent observations have found that chromospheric spicules behave like Alfvénic fluctuations. Low-frequency Alfvén waves are predicted to partially reflect in the transition region that has a gradient in the Alfvén speed, thereby producing inward Alfvén waves, which may interact nonlinearly with outward Alfvén waves to generate Alfvénic turbulence. However, the signature of Alfvénic turbulence in the chromosphere has not yet been quantitatively analyzed with observations. Here we analyze some characteristics related to Alfvénic turbulence with the observations from Hinode/SOT. We decompose the height-time diagram of the transverse oscillations to separate the outward and inward propagating Alfvénic-like signals. The counter-propagating waves are found to have similar amplitude, period and phase speed, suggesting a state having an approximate balance in bi-directional energy fluxes. Counter-propagation of intensity oscillation with lower propagation speed is also presented, probably indicating the presence of slow mode waves. Moreover, we attempt to estimate the Elsässer spectra of the chromospheric turbulence for the first time. The relative fluctuations in the magnetic field may be measured as the local slope of wave-like shapes in spicules. The resulting low-frequency Elsässer power spectra look similar to each other without showing a dominant population, which confirms these counter-propagating low-frequency Alfvénic waves are in a state of balanced flux. These observational results are believed to help us better understand the nature of chromospheric turbulence as well as chromospheric heating.

Key words: Sun: chromosphere — turbulence — solar wind

1 INTRODUCTION

How the processes of heating the solar corona and accelerating the solar wind occur remain completely unsolved. The Alfvén wave, a general kind of magnetohydrodynamic wave, and corresponding Alfvénic turbulence are considered to be crucial for heating and acceleration of solar wind (Tu & Marsch 1995). As the source of coronal energy, an Alfvén wave is probably generated from the region of strong, complex magnetic fields like the boundaries of supergranules that arise from small scale magnetic reconnection (Axford & McKenzie 1992). The upward-propagation, evolution and dynamical effects of Alfvén waves in the chromosphere, transition region and corona have been

* Supported by the National Natural Science Foundation of China.

theoretically described by Hollweg (1982) and Hollweg (1992). The Alfvén waves in the frequency range between 1 Hz and 1 kHz may enter and heat the corona by dissipation near the gyrofrequency (Tu & Marsch 1997; Chen & Hu 2001; Li et al. 2004; He et al. 2008). However, the low-frequency upward waves may strongly reflect in the transition region where there is a large gradient in Alfvén speed and thus produce downward waves (Suzuki & Inutsuka 2005). Then the upward and downward waves interact nonlinearly, triggering and sustaining a perpendicular turbulent cascade across the mean magnetic field (Matthaeus et al. 1999; Dmitruk et al. 2002). Even though the low-frequency Alfvén waves may be strongly reflected in the transition region, the residual amount of energy carried by them to the corona is much more than that carried by high-frequency Alfvén waves, which makes people scrutinize low-frequency waves when studying the problem of coronal heating and acceleration of the solar wind.

Signatures of Alfvén waves (e.g., transverse oscillations) were observationally identified in both the chromosphere and the corona. Using the observations from Hinode/SOT, De Pontieu et al. (2007) detected Alfvén waves in the chromosphere with oscillation speeds of $10\text{--}25\text{ km s}^{-1}$ and periods of $100\text{--}500\text{ s}$, leading to speculation that these waves carry enough energy to accelerate the solar wind and probably heat the quiet corona. A clear signature of upward propagation of relatively high-frequency Alfvén waves was reported by He et al. (2009b). Further study made by He et al. (2010b) showed that there are not only upward but also downward propagating waves moving along spicules. Okamoto & De Pontieu (2011) did a statistical study of Alfvén waves moving along spicules in a southern polar coronal hole, showing that there are three types of waves, upward propagating (59%), downward propagating (21%) and standing (20%) waves. Generation of Alfvén waves by magnetic reconnection in the chromosphere was also observed by SOT (He et al. 2009a). Torsional Alfvén waves in the chromosphere are also claimed to exist based on observations (Jess et al. 2009). Tomczyk et al. (2007) identified Alfvén waves propagating in the corona with observations from a Coronal Multi-Channel Polarimeter, which has the ability to clearly show the oscillations in Doppler shift off the limb. Moreover, the Alfvén waves in the transition region and corona are found in observations from the instrument AIA onboard the spacecraft *Solar Dynamics Observatory* (McIntosh et al. 2011). However, the characteristics of Alfvénic turbulence have not yet been observationally analyzed.

Alfvén waves can steepen into a fast shock and drive upflows like spicules (Hollweg 1982), rapidly evolving elongated jet-like features, ubiquitous in the chromosphere (Xia et al. 2005), which are usually considered to be related to coronal heating and the origin of the solar wind. The shocks produced by a sudden enhancement in pressure passing through the chromosphere push the matter upward (Suematsu et al. 1982). Kudoh & Shibata (1999) studied the properties of spicules and Alfvén waves, finding that the generation of spicules is due to both fast waves and slow waves. An advanced study based on a shock model of the spicules considering the p-modes found that the upward propagation that occurs in acoustic shocks may be generated from photospheric flows and oscillations (De Pontieu et al. 2004). Additionally, based on the observations from SOT, the spicules have been studied statistically and divided into at least two types, type-I and type-II (de Pontieu et al. 2007). Both types of spicules carry Alfvén waves with large velocity amplitudes of 20 km s^{-1} , which may be important for coronal heating (de Pontieu et al. 2007). However, by restudying the same datasets adopted by de Pontieu et al. (2007) with a different analysis method, Zhang et al. (2012) found that the type-I spicules are more dominant and the heating mechanism of type-II spicules should be considered carefully. As an important phenomenon, acoustic waves were observed in the form of a bright structure that was propagating upward in solar polar plumes (Deforest & Gurman 1998). Wang et al. (2009) identified the slow mode waves in the solar atmosphere with optical spectral observations from Hinode/EIS. A comprehensive review of magneto-acoustic waves in the solar atmosphere was given by Nakariakov & Verwichte (2005). Recently the propagation of an intensity disturbance was also argued to be a possible signature of intermittent upflows (e.g., He et al. 2010a; Tian et al. 2011).

In this article, we investigate the Alfvénic waves and related turbulence in the chromosphere using Hinode/SOT observations. In Section 2, we will describe the data processing method. In Section 3, we will show the height-time diagram of the transverse oscillations and intensity oscillations and extract the outward (upward) and inward (downward) propagations of both oscillations by performing a Fourier transform. Analyzing and comparing the characteristics of these two counter-propagations, we find that bi-directional propagation may be in a state that is almost balanced. In Section 4, we will give the estimation of the Elsässer spectra for the chromospheric turbulence, which also shows a balanced state of outward and inward Alfvén waves. Finally, the conclusion and discussion will be given in Section 5.

2 IMAGE PROCESSING-OUTLINING CHROMOSPHERIC SPICULES

The datasets we used were obtained from Hinode/SOT observations on 2011 June 16 in the Ca II H (3968 Å) line. During this period, SOT was staring at the southern limb in a region that had a coronal hole with a cadence of 1.6 s and an exposure time of 0.614 s. The spatial size of a pixel was 0.11". The procedure "fg_prep.pro," available in Solar Software, was used to reduce the data and most of the jitter between images was removed by performing Fourier cross-correlation. Then the coordinate of each image was reset by limb-fitting. The normal radial gradient filtering (NRGF) method (Morgan et al. 2006) was applied to enhance the visibility of the limb structure and then we successively smoothed every three pictures. With the Octodirectional Maxima of Convexities (OMC) method (Koutchmy & Koutchmy 1989), we enhanced the information about the structure by choosing the maximum value of the second derivatives in eight directions relative to each pixel to sharpen the image. An example of the original image, image after NRGF, and image after OMC are illustrated in the left, middle and right panels of Figure 1 respectively.

Furthermore, IDL functions "erode" and "dilate" were applied to refine the spicules' shapes. Then the IDL function "thin" was used to compute rough skeletons of the spicules. Finally, four cases were chosen for further analysis according to the following rules (Okamoto & De Pontieu 2011): (1) the length of each spicule should be more than 4"; (2) the maximum length of each spicule was required to be longer than 8"; (3) the lifetime of each spicule had to be more than 40 s. Based on the spicule skeleton that roughly resulted from the function "thin," we calculated an accurate x-coordinate of the spicules' centroids at given heights by performing an intensity-weighted average. The centroids at every height are marked as red crosses in Figure 2. An animation illustrating the evolution of the case-4 spicule is available from online materials.

3 SEPARATION AND ANALYSIS OF UPWARD AND DOWNWARD PROPAGATIONS

From the height-time diagram of transverse displacement, we can see some background information, because the spicules are slightly tilted and slowly oscillate as a whole. The background information we removed in the diagram represents the parts with zero frequency or zero wave number in the Fourier-transformed spectrum of the height-time diagram which is irrelevant to the upward and downward propagation ($\omega \neq 0, k \neq 0$). Therefore, our step to remove the background is equivalent to setting the spectrum at $\omega = 0$ or $k = 0$ to be zero, without introducing artificial oscillations. To fulfill this criterion, at every point (e.g. time = t_0 , height = h_0) of the height-time diagram we subtracted the time-averaged value at height = h_0 and the height-averaged value at time = t_0 , leaving the information only related to upward and downward propagations. Afterwards, a two-dimensional (2D) Fourier transform was applied to the height-time diagram, yielding a spectral diagram in (ω, k) space. Finally, we performed a 2D inverse Fourier transform using only the first and third quadrants of the (ω, k) diagram, obtaining the upward propagation. Likewise, the second and fourth quadrants were used in a 2D inverse Fourier transform to obtain the downward propagation.

With the spicules' centroids at every height, we acquired the height profile of the original radiation intensity for the spicules' skeleton. There is also background information, because the intensity

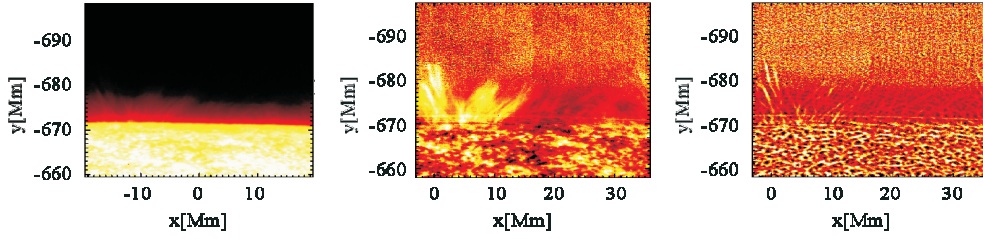


Fig. 1 Original image (*left panel*) from SOT, corresponding images after NRGF (*middle panel*) and after NRGF as well as OMC (*right panel*) are given here for comparison.

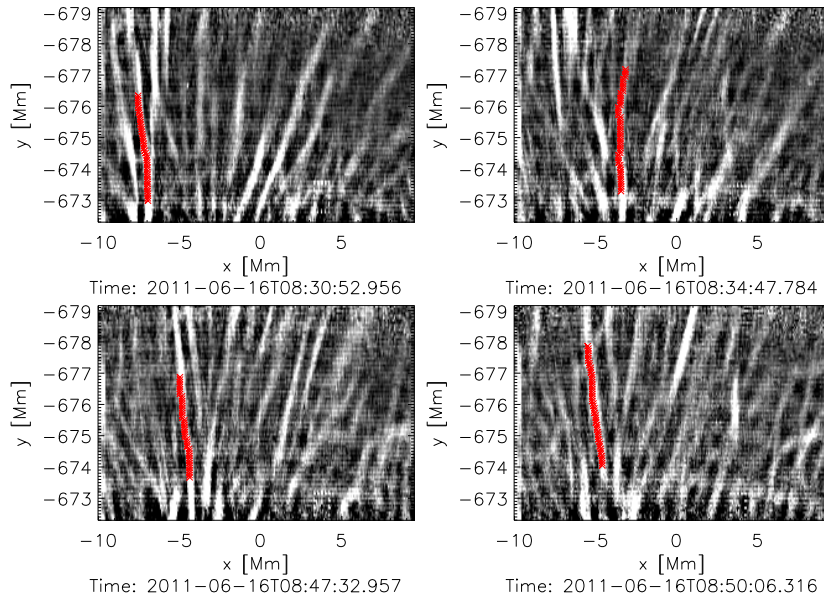


Fig. 2 The spicules in case-1 (*top left panel*), case-2 (*top right panel*), case-3 (*bottom left panel*) and case-4 (*bottom right panel*) are presented. The centroids of each spicule within certain height intervals are marked as red crosses.

oscillates and becomes weaker with increasing height. Then we employed a similar method as was done for the height-time diagrams of transverse displacement to analyze the characteristics of propagating disturbance of intensity, which can be identified as the slow acoustic wave. Four cases are studied here. Their results are generalized in Table 1. Moreover, we applied the same method to pure noise and the results show that there are no obvious signals of upward or downward propagation. To verify the reliability of the observed propagating signal, we mix the height-time diagram of transverse displacement with noise (noise level: from 0.1 to 0.5 spatial pixels). The test results indicate that the upward and downward signals still exist without being heavily contaminated by noise. Therefore, we consider our result to be believable.

For the first spicule, the upward and downward propagations of transverse oscillation seem to be quasi-periodic with periods of both being approximately 110 s (see top panels of Fig. 3). The upward speed is roughly 70 km s^{-1} and the downward speed is around 30 km s^{-1} . Besides these, the amplitude of upward propagation is a little larger than that of downward propagation.

Table 1 Upward and Downward Propagation of Transverse Oscillation and Intensity Oscillation

		Transverse oscillation				Intensity oscillation		
		V_{pro} (km s^{-1})	Period (s)	Displacement Amplitude (km)	Velocity Amplitude (km s^{-1})	V_{pro} (km s^{-1})	Period (s)	Amplitude (Arb-Unit)
Case-1	Upward	70	~ 110	49	2.8	30	–	8.6
	Downward	30	~ 110	40	2.3	20	~ 100	7.5
Case-2	Upward	40	~ 100	76	4.8	10	–	5.3
	Downward	40	~ 100	56	3.5	10–20	–	6.0
Case-3	Upward	60–70	~ 50	67	8.4	40	–	8.8
	Downward	20–30	–	65	–	30	–	6.5
Case-4	Upward	130	~ 100	56	3.5	20	–	7.1
	Downward	30	–	46	–	20	–	3.5

Notes: 1. V_{pro} represents the propagation speed of the identified transverse oscillation or intensity oscillation. 2. Arb-Unit stands for arbitrary unit.

In case-1, the periodicity of upward propagation of intensity oscillation is not obvious but the period of downward propagation of intensity oscillation seems to be 100 s (see bottom panels of Fig. 3). The upward speed is almost 30 km s^{-1} and the downward speed is around 20 km s^{-1} . The amplitude of upward propagation is also a little larger than that of downward propagation.

For the second case of Alfvénic fluctuations (see top panels of Fig. 4), both the upward and downward propagations are identified to be quasi-periodic at nearly 100 s with a speed of about 40 km s^{-1} . The amplitude of upward propagation seems to be a little greater than that of downward propagation. It is hard to identify the periodicity for the intensity disturbance of case-2. For the intensity disturbance (see bottom panels of Fig. 4), the upward propagation speed is around 10 km s^{-1} and the downward speed changes from 10 to 20 km s^{-1} . The upward propagating intensity disturbance is slightly weaker than that of the downward propagation.

For case-3 as illustrated in Figure 5, the transverse oscillation propagates upward with a shorter period (50 s) at first and then the periodicity becomes unobvious. Also, the downward propagation period is difficult to identify. The upward speed ranges between 60 and 70 km s^{-1} and the downward speed varies from 20 to 30 km s^{-1} . The amplitude of upward propagation is roughly the same as that of the downward propagation. Like case-2, it is also difficult to discern the periodicity of upward and downward propagations for the intensity oscillation of case-3. The upward speed is more or less 40 km s^{-1} and the downward speed is roughly 30 km s^{-1} . The intensity of the signal for upward propagation seems to be a little stronger than that of downward propagation.

For the fourth spicule as shown in Figure 6, the period of upward propagation is roughly 100 s, but the downward propagation is hard to identify. The upward speed is nearly 130 km s^{-1} and the downward speed is around 30 km s^{-1} . The amplitude of upward propagation is also a little greater than that of downward propagation. There seems to be no obvious periodicity for the upward and downward propagations of intensity oscillation in case-4. The upward and downward speeds are both around 20 km s^{-1} . The amplitude of upward propagation is greater than that of downward propagation.

4 ESTIMATION OF THE ELSÄSSER SPECTRUM

The Elsässer variable is an important parameter to describe MHD turbulence, defined as $z_{\pm} = v \pm b/(4\pi\rho)^{1/2}$, where v is the velocity fluctuation, b is the magnetic field fluctuation and ρ is the

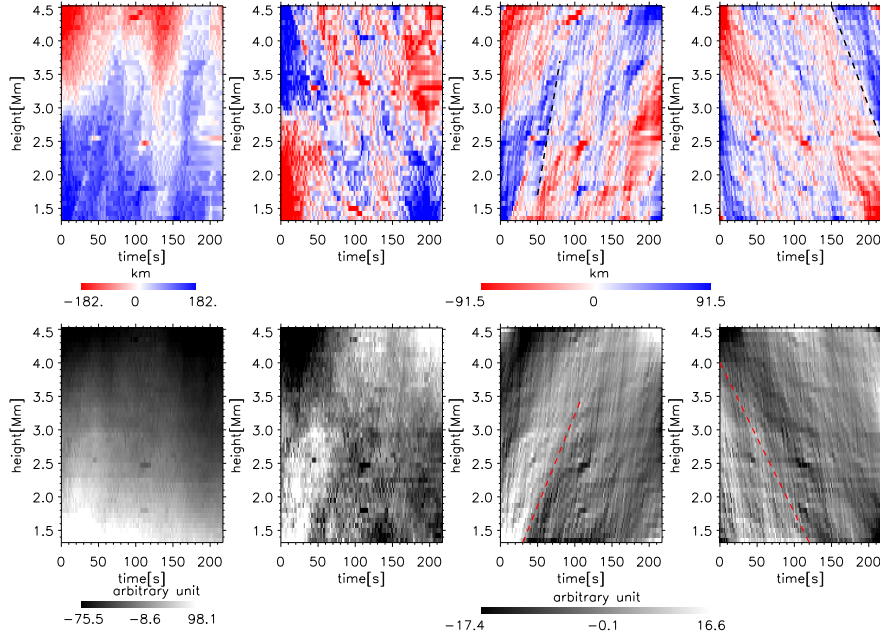


Fig. 3 Case-1. The upper four panels give the height-time diagrams (original diagram, composite without background, only upward propagation and only downward propagation) of the transverse oscillation respectively (*from left to right*). The lower four panels describe the height-time diagrams (original diagram, composite without background, only upward propagation and only downward propagation) of intensity oscillation respectively (*from left to right*). The dashed lines represent the direction of propagation.

density of plasma. The difficulty of estimating Elsässer variables in the solar atmosphere lies in that it is impossible to directly obtain the magnetic field fluctuation and the plasma density. We thus adopt an indirect method. We substitute $V_A = B/\sqrt{4\pi\rho}$ for $\sqrt{4\pi\rho}$ into the definition for the Elsässer variable, and then we obtain the expression $z_{\pm} = v \pm V_A b/B$, where V_A is the Alfvén speed and B is the background magnetic field intensity. Though it is hard to directly calculate b and B from observations, b/B may be measured as the local slope of spicules' shape, i.e. $\delta x/\delta y$. However, in an ideal state, $V_A = \pm vB/b$, so V_A may be represented as the ratio of the variance of speed to the variance of slope. This kind of V_A estimation seems to be more appropriate than estimating from propagation speed, which accounts for the composite effect of both plasma flow and wave propagation.

Therefore, the estimation of the Elsässer spectrum becomes an estimation of Alfvén speed and spicule slope. When estimating the Alfvén speed and spicule slope, one should consider the interval of time and height. According to the expressions, $v = (x_1 - x_2)/\Delta t$ and $b/B = (x_1 - x_2)/\Delta y$, we can derive the respective equations for error propagation, $\sigma_v = \sqrt{(e_1^2 + e_2^2)}/\Delta t$ and $\sigma_{b/B} = \sqrt{(e_1^2 + e_2^2)}/\Delta y$, where Δt is the time interval and Δy is the height interval; e_1 and e_2 are errors in the x coordinates at either two different times or different heights which we assume to be 0.1 pixel (i.e. $0.01''$, 7 km). Thus if σ_v is less than $0.2v$, which is about 2 km s^{-1} , we need Δt to be greater than 4.9 s. When $\sigma_{b/B}$ is less than $0.2b/B$ which can be estimated to be $0.2v/V_A$ (~ 0.02), Δy is required to be larger than $0.7''$. Additionally, since V_A is much larger than v , the sensitivity of the Elsässer spectrum to the height interval is more significant than that to the time interval.

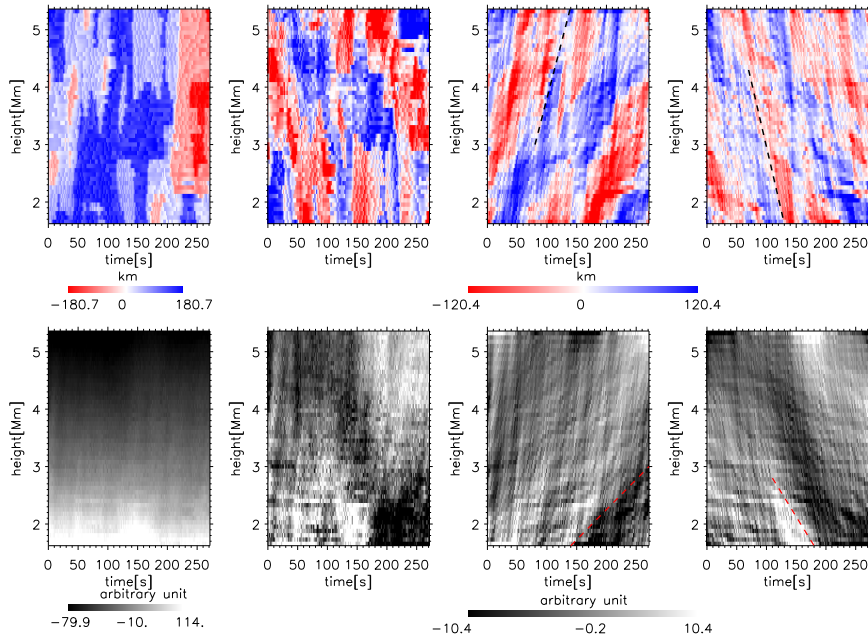


Fig. 4 Case-2. The upper four panels give the height-time diagrams (original diagram, composite without background, only upward propagation and only downward propagation) of the transverse oscillation respectively (*from left to right*). The lower four panels describe the height-time diagrams (original diagram, composite without background, only upward propagation and only downward propagation) of intensity oscillation respectively (*from left to right*). The dashed lines denote the tendency of propagation.

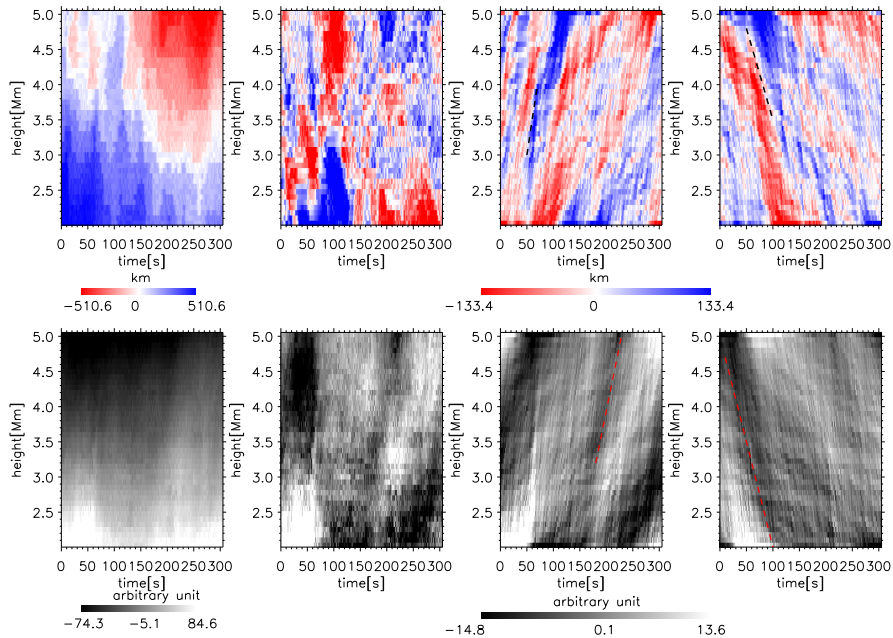


Fig. 5 Case-3. The meaning of every panel is the same as that for case-2 in Fig. 4.

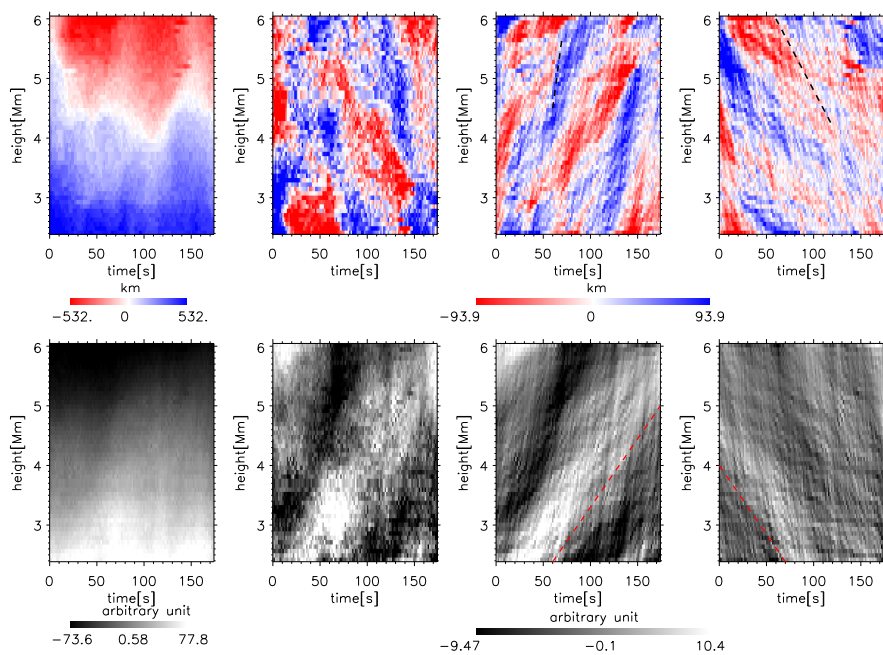


Fig. 6 Case-4. The meaning of every panel is the same as that for case-2 in Fig. 4.

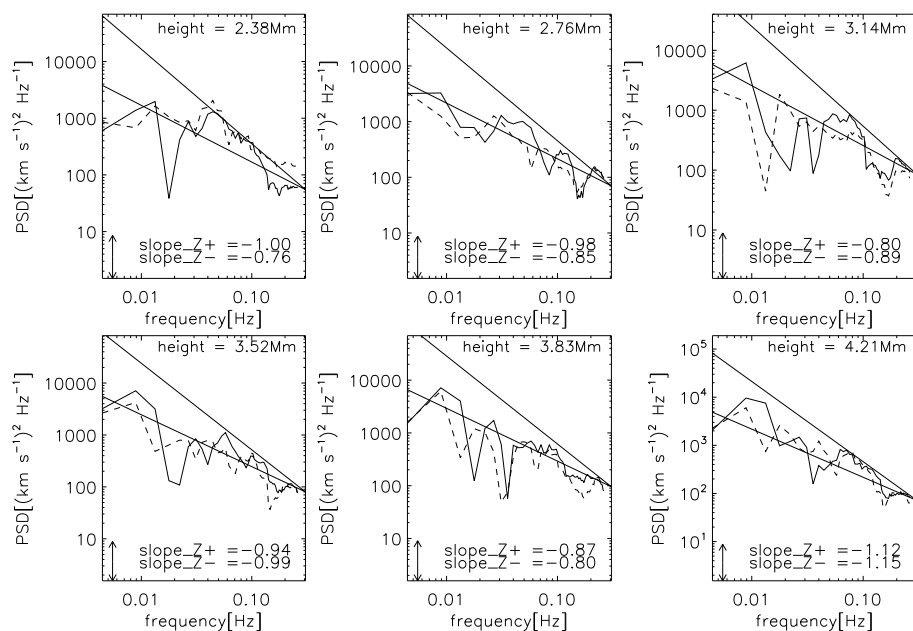


Fig. 7 Case-1. The spectra of Z+ (*solid line*) and Z- (*dashed line*) at six different heights: 2.38, 2.76, 3.14, 3.52, 3.83 and 4.21 Mm, showing that the spectra of Z+ and Z- are similar in terms of power level. The two straight black lines with a slope of -1 and $-3/5$ are plotted to compare them with the spectral slopes.

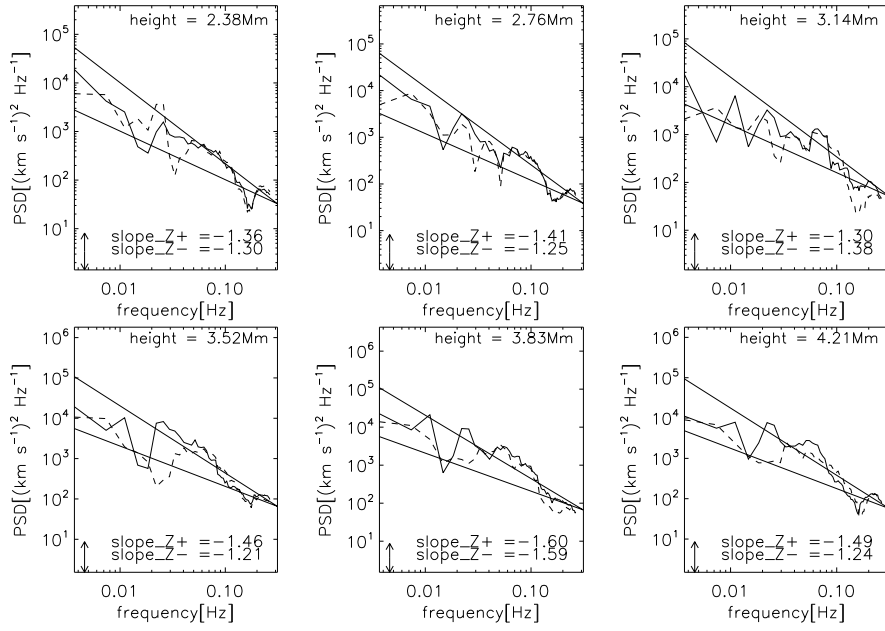


Fig. 8 Case-2. The spectra of Z+ (*solid line*) and Z- (*dashed line*) at six different heights: 2.38, 2.76, 3.14, 3.52, 3.83 and 4.21 Mm, showing that the spectra of Z+ and Z- are similar. The two straight black lines with the slope of -1 and $-3/5$ are plotted to compare them with the spectral slopes.

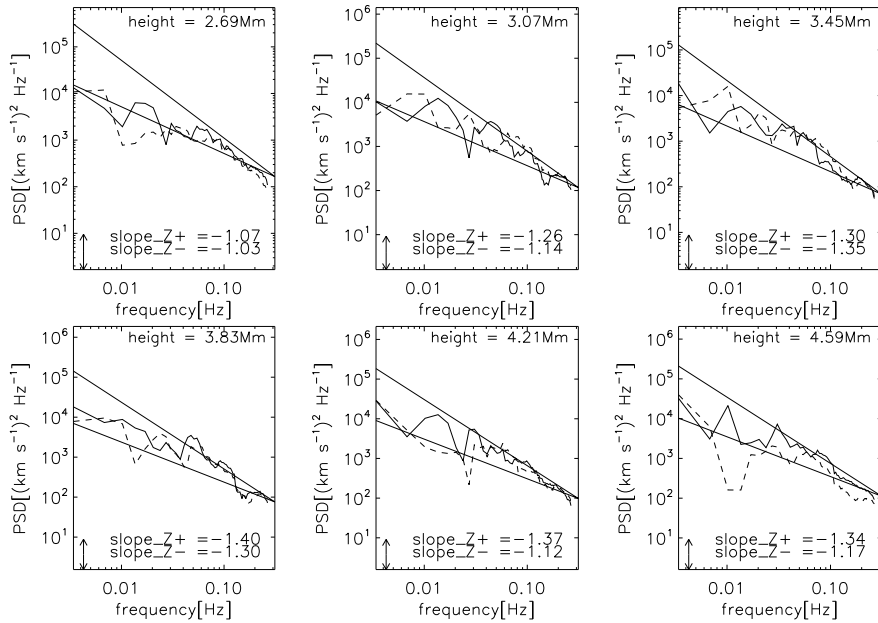


Fig. 9 Case-3. Every panel has the same meaning as that for case-2 in Fig. 8.

Table 2 Elsässer Power Spectrum at Different Heights

Case-1	Height (Mm)	2.38	2.76	3.14	3.52	3.83	4.21
	Z+ Slope	-1.00	-0.98	-0.80	-0.94	-0.87	-1.12
	Z- Slope	-0.76	-0.85	-0.89	-0.99	-0.80	-1.15
	Z+ rms (km s ⁻¹)	14.5	13.8	15.6	15.8	20.1	24.8
	Z- rms (km s ⁻¹)	15.5	13.4	13.9	14.3	18.7	23.1
Case-2	Height (Mm)	2.38	2.76	3.14	3.52	3.83	4.21
	Z+ Slope	-1.36	-1.41	-1.30	-1.46	-1.60	-1.49
	Z- Slope	-1.30	-1.25	-1.38	-1.21	-1.59	-1.24
	Z+ rms (km s ⁻¹)	12.8	14.5	14.2	18.7	21.0	17.0
	Z- rms (km s ⁻¹)	11.4	11.8	11.2	14.4	17.0	13.8
Case-3	Height (Mm)	2.69	3.07	3.45	3.83	4.21	4.59
	Z+ Slope	-1.11	-1.30	-1.34	-1.35	-1.30	-1.36
	Z- Slope	-1.05	-1.19	-1.29	-1.20	-1.15	-1.19
	Z+ rms (km s ⁻¹)	45.7	50.5	38.5	37.6	34.4	24.9
	Z- rms (km s ⁻¹)	47.1	52.1	40.1	38.0	33.9	22.9
Case-4	Height (Mm)	3.07	3.37	3.75	4.13	4.44	4.82
	Z+ Slope	-0.88	-0.92	-0.93	-1.13	-1.20	-0.87
	Z- Slope	-0.59	-0.77	-0.65	-0.77	-0.98	-0.99
	Z+ rms (km s ⁻¹)	57.8	62.5	55.4	55.6	35.5	56.4
	Z- rms (km s ⁻¹)	57.9	62.7	55.4	55.0	35.4	56.8

The sensitivity of the Elsässer spectrum to the height interval is more obvious (indicating more uncertainty in spectral estimation) when the height interval is less than $1.1''$, which is close to the lower limit $0.7''$ ($\Delta y_{\min} \sim 0.7''$). In addition, the sensitivity to time difference is relatively stable when the time interval is larger than 4.8 s. Considering the lower limit of the height interval and the time interval, the stability of the Elsässer spectrum and the length of a spicule, we finally set the height interval to be $2.2''$ and the time interval to be 6.4 s. With these intervals, we derive the Elsässer variables at different heights and different times.

Then we estimate the Elsässer power spectra at different heights (see Figs. 7, 8, 9 and 10 for Elsässer power spectra of cases 1, 2, 3 and 4) with their power law index shown in Table 2. In sum, the slope of each power spectrum is near -1 , which deviates from Kolmogorov's power law, and shows no obvious change with height. Moreover, neither $Z+$ nor $Z-$ is in a dominant state indicating that the counter-propagating low-frequency Alfvénic waves are in a quasi-balanced state of energy flux.

5 SUMMARY AND DISCUSSION

As far as we know, this is the first attempt to investigate chromospheric Alfvénic turbulence from observations. Our study shows the following results.

- (1) A low-frequency (about 0.01 Hz) chromospheric Alfvén wave has the characteristics of upward and downward propagation. The upward speed is almost 70 km s^{-1} and the downward speed is relatively less, probably due to some upflow. Additionally, the amplitude of upward propagation

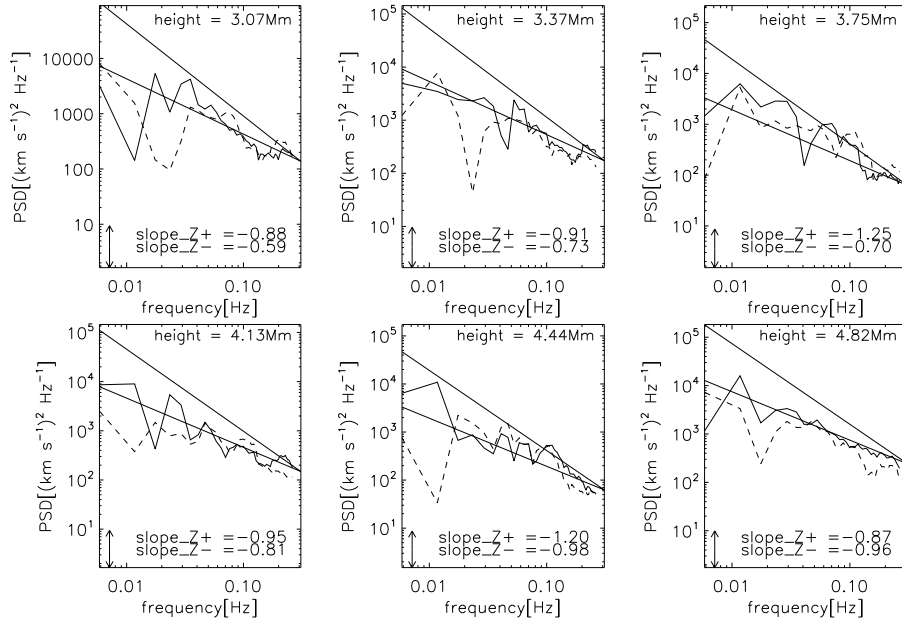


Fig. 10 Case-4. Every panel has the same meaning as that for case-2 in Fig. 8.

is more or less the same as that of downward propagation. The velocity amplitudes of transverse motion are around $3\text{--}8\text{ km s}^{-1}$ which is consistent with the result of Okamoto & De Pontieu (2011) ($7.4 \pm 3.7\text{ km s}^{-1}$).

- (2) The intensity oscillation, probably a slow acoustic wave, has a longer period and a slower propagation speed than that of transverse oscillation. Moreover, the amplitude of upward propagation is also similar to that of downward propagation.
- (3) The power spectra of Z+ and Z- look alike. Their slopes are both near -1 implying that the chromospheric turbulent flux is in a balanced state.

The exact estimation of Elsässer variables still has some difficulties. First, the estimation of Alfvén speed is not quite stable, which might dramatically change at different heights. If possible, the accuracy of estimating Alfvén speed needs to be improved. Second, there is no strict rule to determine the span of time and height while estimating the fluctuation speed and the local slope of spicules' shape. Hence, the results may vary due to the different time or height intervals. Fortunately, the sensitivity of the change at different intervals we choose is relatively small. Third, due to the short lifetime of spicules and the discrete observations with certain time resolution, the number of the images of the chosen spicules is limited even though the lifetime of spicules we choose is relatively long. Though there are numerous spicules during the time we consider, spicules that are easy for us to trace for a long enough time are rare. Some spicules disappear in a short time like 40 s, but some spicules may interact or mix with other spicules, which means that it is difficult for us to obtain accurate locations of the spicules. In general, the study of chromospheric Alfvénic turbulence illustrated in this paper sheds new lights on the dynamics of the chromosphere, which is probably useful for our understanding of the nature of chromospheric turbulence as well as the chromospheric heating and acceleration of solar wind.

Acknowledgements We would like to thank C.-Y. Tu, E. Marsch, F.-S. Wei and B. Li for helpful discussions and suggestions. This work is supported by the National Natural Science Foundation

of China (Grant Nos. 41174148, 41222032, 40931055 and 41231069). Z. X. Liu is also supported by the Undergraduate Scientific Research Program of Peking University. J.-S. He is also supported by the Foundation for the Author of National Excellent Doctoral Dissertation of PR China (Grant No. 201128).

References

- Axford, W. I., & McKenzie, J. F. 1992, in *Solar Wind Seven Colloquium, The Origin of High Speed Solar Wind Streams*, eds. E. Marsch, & R. Schwenn, 1
- Chen, Y., & Hu, Y. Q. 2001, *Sol. Phys.*, 199, 371
- De Pontieu, B., Erdélyi, R., & James, S. P. 2004, *Nature*, 430, 536
- de Pontieu, B., McIntosh, S., Hansteen, V. H., et al. 2007, *PASJ*, 59, 655
- De Pontieu, B., McIntosh, S. W., Carlsson, M., et al. 2007, *Science*, 318, 1574
- Deforest, C. E., & Gurman, J. B. 1998, *ApJ*, 501, L217
- Dmitruk, P., Matthaeus, W. H., Milano, L. J., et al. 2002, *ApJ*, 575, 571
- He, J.-S., Tu, C.-Y., & Marsch, E. 2008, *Sol. Phys.*, 250, 147
- He, J., Marsch, E., Tu, C., & Tian, H. 2009a, *ApJ*, 705, L217
- He, J.-S., Tu, C.-Y., Marsch, E., et al. 2009b, *A&A*, 497, 525
- He, J.-S., Marsch, E., Tu, C.-Y., Guo, L.-J., & Tian, H. 2010a, *A&A*, 516, A14
- He, J.-S., Marsch, E., Tu, C.-Y., & Tian, H. 2010b, *Twelfth International Solar Wind Conference*, 1216, 32
- Hollweg, J. V. 1982, *ApJ*, 257, 345
- Hollweg, J. V. 1992, *ApJ*, 389, 731
- Jess, D. B., Mathioudakis, M., Erdélyi, R., et al. 2009, *Science*, 323, 1582
- Koutchmy, O., & Koutchmy, S. 1989, *Optimum Filter and Frame Integration Application to Granulation Pictures*, in *High Spatial Resolution Solar Observations*, ed. O. von der Luehe, 217
- Kudoh, T., & Shibata, K. 1999, *ApJ*, 514, 493
- Li, B., Li, X., Hu, Y.-Q., & Habbal, S. R. 2004, *Journal of Geophysical Research (Space Physics)*, 109, A07103
- Matthaeus, W. H., Zank, G. P., Oughton, S., Mullan, D. J., & Dmitruk, P. 1999, *ApJ*, 523, L93
- McIntosh, S. W., de Pontieu, B., Carlsson, M., et al. 2011, *Nature*, 475, 477
- Morgan, H., Habbal, S. R., & Woo, R. 2006, *Sol. Phys.*, 236, 263
- Nakariakov, V. M., & Verwichte, E. 2005, *Living Reviews in Solar Physics*, 2, 3
- Okamoto, T. J., & De Pontieu, B. 2011, *ApJ*, 736, L24
- Suematsu, Y., Shibata, K., Neshikawa, T., & Kitai, R. 1982, *Sol. Phys.*, 75, 99
- Suzuki, T. K., & Inutsuka, S.-i. 2005, *ApJ*, 632, L49
- Tian, H., McIntosh, S. W., & De Pontieu, B. 2011, *ApJ*, 727, L37
- Tomeczyk, S., McIntosh, S. W., Keil, S. L., et al. 2007, *Science*, 317, 1192
- Tu, C.-Y., & Marsch, E. 1995, *Space Sci. Rev.*, 73, 1
- Tu, C.-Y., & Marsch, E. 1997, *Sol. Phys.*, 171, 363
- Wang, T. J., Ofman, L., Davila, J. M., & Mariska, J. T. 2009, *A&A*, 503, L25
- Xia, L. D., Popescu, M. D., Doyle, J. G., & Giannikakis, J. 2005, *A&A*, 438, 1115
- Zhang, Y. Z., Shibata, K., Wang, J. X., et al. 2012, *ApJ*, 750, 16